# iNEMI Pb-FREE ALLOY CHARACTERIZATION PROJECT REPORT: PART II - THERMAL FATIGUE RESULTS FOR TWO COMMON TEMPERATURE CYCLES

Richard Parker[1], Richard Coyle[2], Gregory Henshall[3], Joe Smetana[4], Elizabeth Benedetto[5]
[1]Delphi, Kokomo, IN, USA
[2]Alcatel-Lucent, Murray Hill, NJ, USA
[3]Hewlett-Packard Co., Palo Alto, CA, USA
[4]Alcatel-Lucent, Plano, TX, USA
[5]Hewlett-Packard Co., Houston, TX, USA
richard.d.parker@delphi.com; richard.coyle@alcatel-lucent.com

**ABSTRACT**
The Pb-Free Alloy Characterization Program sponsored by International Electronics Manufacturing Initiative (iNEMI) is conducting an extensive investigation using accelerated temperature cycling (ATC) to evaluate ball grid array (BGA) thermal fatigue performance of 12 commercial or developmental Sn based Pb-free solder alloys. This paper presents the initial findings from a specific subset of the temperature cycling test matrix. The focus is on comparing alloy performance for two of the most commonly specified temperature cycles, 0 to 100 °C and -40 to 125 °C. These two cycles have different temperature extremes and cyclic temperature ranges (referred to as $\triangle T$) but identical 10 minute hot and cold dwell times. The failure data are reported as characteristic life $\eta$ (number of cycles to 63.2% failure) and slope $\beta$ from a two-parameter Weibull analysis. The ATC data and failure analyses are discussed in terms of the relationship to alloy composition and to the initial microstructures as well as the microstructures as they evolve during temperature cycling.

Key words: Pb-free solder, thermal fatigue, accelerated temperature cycling

**INTRODUCTION**
Innovations in Sn based Pb-free solder alloy development are being driven by volume manufacturing and field experiences. As a result, there has been an increase in the number of Pb-free solder alloy choices beyond the common near-eutectic Sn-Ag-Cu (SAC) alloys first established as replacements for Sn-Pb. The development of Pb-free alloys provides opportunities to address shortcomings of the high Ag, near-eutectic SAC, such as the poor mechanical shock performance, alloy cost, copper dissolution of plated through holes, and poor mechanical behavior of joints during board bending. At the same time, the increase in alloy choice introduces a variety of technical risks, such as a potential decrease in thermal fatigue resistance [1, 2]. Thermal fatigue and creep performance is critically important for high reliability applications because it is a major source of failure of surface mount (SMT) components [3]. For Pb-free alloys, the processes of microstructural aging, creep, and thermal fatigue are known to be dependent on the alloy composition, particularly the Ag content [4-9], which is one of the principal variables in the iNEMI test matrix.

Accelerated thermal cycling (ATC) is the standard method for assessing susceptibility to low cycle, thermal fatigue failure. The thermal fatigue reliability of Pb-free solders is sensitive to temperature cycling parameters such as dwell time and temperature extremes but it has received limited treatment in the literature compared to eutectic Sn-Pb solder [10]. This paper presents the initial temperature cycling results for multiple Pb-free solder alloys from the iNEMI matrix using two of the most commonly specified temperature cycles, 0 to 100 °C and -40 to 125 °C. The former cycle is used typically for telecommunication information technology applications and the latter is used for harsher use environments such as automotive. The test results and failure analyses are discussed in terms of the relationship to Ag content and dopant content, differences in acceleration factor between the two temperature cycles, and to the initial as well as evolving microstructures during temperature cycling.

**EXPERIMENTAL**
Detailed descriptions of the iNEMI Pb-Free Alloy Characterization program goals, experimental plan, and test protocols are provided in previous publications [11, 12]. The test program is in progress and includes 12 commercial or developmental Sn based Pb-free solder alloys, a eutectic Sn-37Pb solder baseline, two different ball grid array (BGA) components, and 10 different temperature cycles for studying thermal fatigue behavior. The results for the temperature cycling subset presented here include data for the two the BGA components fabricated with five different commercial Pb-free alloys: SAC405 SAC305, SAC205, SAC105, and SN100C and a Sn-37Pb eutectic alloy baseline. The nominal alloy compositions are shown in Table 1.

**Test Vehicle**
Figure 1 shows a fully populated iNEMI Alloy Characterization BGA test vehicle. Each printed circuit board assembly (PCBA) contains a total of 32 components,

with 16 of the larger 192CABGA component and 16 of the smaller 84CTBGA component. The attributes of the BGA components and printed circuit board (PCB) test vehicle are shown in Table 2. The parts were procured as land grid arrays (LGA) to enable subsequent attachments of the various different solder alloy balls [12].

**Table 1:** Nominal solder alloy compositions used in this test matrix.

| Alloy | Nominal Composition* (wt. %) | | | |
|---|---|---|---|---|
| | Sn | Ag | Cu | other |
| SAC405 | 95.5 | 4.0 | 0.5 | |
| SAC305 | 96.5 | 3.0 | 0.5 | |
| SAC205 | 97.5 | 2.0 | 0.5 | |
| SAC105 | 98.5 | 1.0 | 0.5 | |
| SN100C | 99.3 | 0.0 | 0.7 | Ni<0.1, Ge trace |
| SnPb | 63.0 | | | 37.0 Pb |

*analyzed compositions provided in ref. [12]

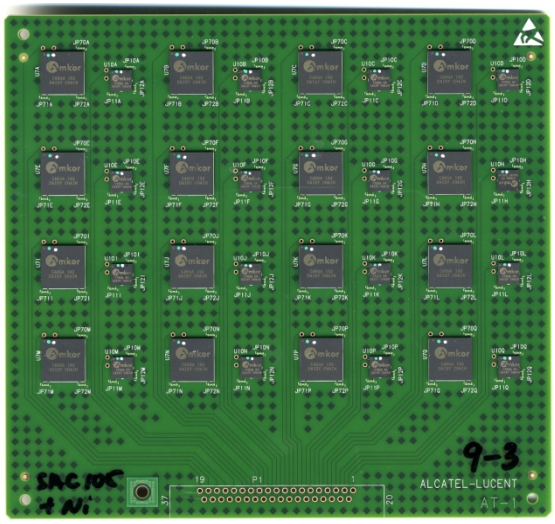


**Figure 1: A** fully populated iNEMI Alloy Characterization test vehicle with the larger 192 CABGA and the smaller is 84CTBGA component.

**Table 2:** Attributes of the ball grid array (BGA) and printed circuit board (PCB) test vehicles.

| BGA Package | | |
|---|---|---|
| Designation | 192CABGA | 84CTBGA |
| Die Size | 12x12 mm | 5x5 mm |
| Package Size | 14x14 mm | 7x7 mm |
| Ball Array | 16x16 | 12x12 |
| Ball Pitch | 0.8 mm | 0.5 mm |
| Ball Diameter | 0.46 mm | 0.3 mm |
| Pad Finish | Electrolytic Ni/Au | Electrolytic Ni/Au |
| PCB | | |
| Thickness | 2.36 mm (93mils) | |
| Surface Finish | High temp OSP | |
| No. Cu Layers | 6 | |
| Pad Diameter | 0.356 mm | 0.254 mm |
| Solder Mask Dia. | 0.483 mm | 0.381 mm |

**Test Vehicle Assembly**

All of the Pb-free test vehicles were assembled using no clean SAC305 solder paste. The peak temperature for the Pb-free reflow profile was set at 245°C. The SnPb eutectic test vehicle was assembled using Sn-37Pb solder paste with a peak reflow temperature of 215°C. Following assembly, all the cards went through visual inspection, electrical continuity testing, and 5DX x-ray inspection.

**Accelerated Temperature Cycling**

The components and the test circuit boards were daisy chained to allow electrical continuity testing after surface mount assembly and for in situ, continuous monitoring during thermal cycling. The resistance of each loop was independently monitored during the temperature cycle test. The two temperature cycles are described in Table 3. Thermal cycling was done in accordance with the IPC-9701A industry test guideline [13] and the complete testing details are provided in a previous publication [12]. The solder joints were monitored continuously during thermal cycling using an event detector for the 0 to 100 °C test and a data logger for the -40/125 °C test. Both monitoring systems used the same resistance limit of 1000 ohms as described elsewhere [12]. The failure data are reported as characteristic life $\eta$ (the number of cycles to achieve 63.2% failure) and slope $\beta$ from a two-parameter Weibull analysis.

**Table 3:** This table describes the maximum and minimum temperatures and the temperature range, $\triangle T$, for the temperature cycles used in this test.

| Cycle Number | Minimum Temp. (°C) | Maximum Temp. (°C) | Temp. Range (°C) | Dwell Time |
|---|---|---|---|---|
| 1 | 0 | 100 | 100 | 10 |
| 2 | -40 | 125 | 165 | 10 |

**Microstructural Characterization and Failure Analysis**

A baseline characterization was performed on representative printed circuit board assemblies from each test cell. The microstructures were documented before temperature cycling to enable comparisons to failed temperature cycled samples. The analyses were done using optical metallography (destructive cross-sectional analysis) and scanning electron microscopy (SEM). The initial phase identification and elemental analysis was done with energy dispersive spectroscopy (EDS). Subsequent phase differentiation was done using the SEM operating in the backscattered electron imaging (BEI) mode. Optical metallography was the primary tool used to verify the failure mode. Although optical metallography typically is adequate for Sn-37Pb solder assessments, the SEM used in the backscattered electron imaging (BEI) mode is known to be particularly useful for differentiating phases in the SAC microstructures.

## RESULTS AND DISCUSSION

### Microstructural Characterization

Figure 2a and Figure 2b show high magnification backscattered electron images (original magnification 2000X) comparing the baseline (prior to thermal cycling) BGA solder joint microstructures for each of the five Pb-free alloys and the eutectic Sn-37Pb alloy included in this study (see Table 1). These analyses are performed at relatively high magnification to enable resolution of the fine microstructural features of the Pb-free alloys. Separate images are provided for the 192CABGA and the 84CTBGA packages. This series of micrographs is developed to enable comparisons of the microstructures from surface mount (SMT) assembly to those subsequent to thermal cycling for each of the two package test vehicles and solder ball alloys used in this study. A series of lower magnification optical photomicrographs of SMT assembled samples for each component type and alloy are included in Appendix A.

The large amount of undercooling typically required to nucleate the β–Sn phase tends to suppress the equilibrium ternary eutectic structure in Sn-Ag-Cu Pb-free alloys [14]. This applies to SAC405 and SAC305 despite their near-eutectic composition [15]. Consequently, ternary eutectic decomposition seldom is observed in these microstructures. For the larger 192CABGA component, the microstructures of the four SAC alloys consist of primary Sn cells with secondary $Ag_3Sn$ particles (shown as the lighter phase) at the cell or dendrite boundaries. As expected, the $Ag_3Sn$ particle density increases as the SAC alloy Ag content increases. The SAC405 alloy has the highest Ag content and contains the most $Ag_3Sn$ particles. The undercooling, oversaturation of the Sn with Ag, and local compositional variations combine to cause $Ag_3Sn$ precipitation through a binary eutectic reaction ($L \rightarrow Sn + Ag_3Sn$). In the high Ag alloys the precipitates tend to appear as wider networks or bands along the primary Sn boundaries [4, 5]. Some $Ag_3Sn$ platelets also can be found in the SAC405 alloy balls of the larger 192CABGA component (see Appendix A), most likely the result of slower cooling and solidification with the larger package and solder ball. To a lesser extent, $Ag_3Sn$ banding is found in the SAC305 and SAC205 alloys but the particle densities are lower than with the higher Ag content SAC405.

The $Ag_3Sn$ precipitate density is lowest in the SAC105 alloy and the $Ag_3Sn$ particles are arranged more linearly rather than in wider networks or bands. In addition to having fewer $Ag_3Sn$ particles, the SAC105 also differs from the higher Ag content alloys in that it contains more $Cu_6Sn_5$ intermetallic precipitates (darker phase).

The SN100C, which fundamentally is a Sn-Cu binary alloy with trace additions of certain elements (sometimes called dopants), contains some $Ag_3Sn$ particles resulting from SMT assembly with the SAC305 solder paste. Calculations by the iNEMI project team indicate that assembly with the SAC305 paste creates a Ag content of approximately 0.3 wt. % in the 192CABGA solder balls [12]. Additionally, there are some Au-bearing intermetallic particles present in the assembled SN100C solder balls. Presumably the source of the Au is the BGA component pad surface finish, which is electrolytic Au over electrolytic Ni. The composition and structure of the sub-micron size Au-bearing intermetallic particles could not be determined due to the limitations in spatial resolution of the standard SEM and EDS techniques. Similar Au-bearing particles may be present but less obvious in the other alloys due to the generally higher $Ag_3Sn$ particle density with those alloys.

The microstructures for the 84CTBGA package shown in Figures 2a and 2b differ significantly from those of the larger 192CTBGA package. Variations in particle density similar to those observed in the 192CABGA are expected given the range of Ag content with these alloys. With the 84CTBGA, the $Ag_3Sn$ precipitate density qualitatively seems to be similar in the SAC405, SAC305, and SAC205. This is more likely an artifact from making a qualitative, visual comparison of the images. Quantitative metallography would be required to characterize the particle distribution and density and that is beyond the scope of this work. The primary Sn cell size in the smaller diameter 84CTBGA balls of the SAC alloys is significantly smaller in comparison to the Sn cell size in the larger diameter 192CABGA balls.

The phenomenon referred to as "spalling" was observed in the 84CTBGA package. It was detected only with the SAC205 alloy and it was found in some but not all of the 84CTBGA solder balls. The dark phase in Figure 2a (84CTBGA, SAC205) appears to result from a reaction in which material separates or spalls from the surface of the BGA package pad metallization. Snugovsky et al. have studied this reaction and have indicated that the term spalling is a convenient but incorrect characterization. Their analysis shows that spalling actually results from solidification conditions in the bulk solder rather than at the metallization interface. Those solidification conditions include specific compositional conditions that promote a quasi-peritectic reaction in Sn-based solders in the presence of Cu and Ni [16]. Spalling is an uncommon occurrence, has an unusual morphology, and is located in the region of the solder joint where fatigue cracking propagates. Therefore, it should come as no surprise that spalling creates a general concern that it could affect the performance of solder joints. There are however, no published reports indicating that this spalling phenomenon influences failure mode or thermal fatigue life of SAC solders.

Similar to the case of the 192CABGA, the SAC105 84CTBGA contains more $Cu_6Sn_5$ intermetallic precipitates (darker phase) as well as fewer $Ag_3Sn$ particles. The presence of $Cu_6Sn_5$ is not considered a critical reliability factor in SAC alloys because $Ag_3Sn$ particles are recognized as the primary microstructural strengthening mechanism influencing thermal fatigue resistance in SAC [4, 6, 8, 9, 11]. Compared to the $Ag_3Sn$ particles, the number of $Cu_6Sn_5$ particles is low and they are distributed randomly. Because

the solder ball volume is small, assembly with the SAC305 paste creates a Ag content of approximately 0.8 wt. % in the 84CTBGA solder balls compared to approximately 0.3 wt. % in the larger diameter 192CABGA solder balls [12].

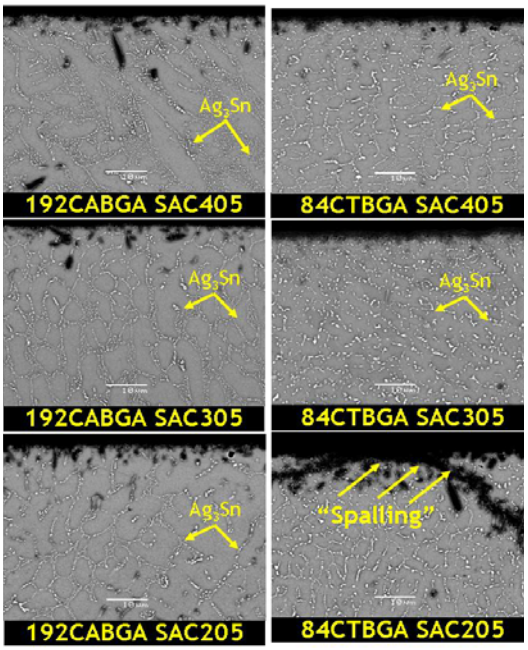


**Figure 2a:** Backscattered electron images of baseline solder joint microstructures for SAC405, SAC305, and SAC205.

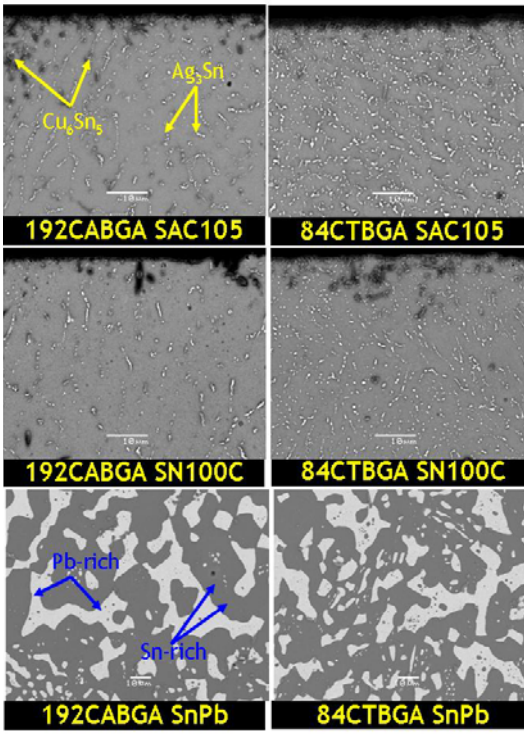


**Figure 2b:** Backscattered electron images of baseline solder joint microstructures for SAC105, SN100C, and eutectic SnPb control.

**ATC Test Results**

The thermal cycling test results are summarized in Tables 4 and 5 and the bar charts in Figures 3 and 4. The data also are shown graphically in the series of Weibull and contour plots presented in Appendix B.

There are a number of notable trends in the thermal cycling data with some following general expectations and others contrary to the anticipated outcome. Before drawing specific comparisons, it should be noted that there are variations in slope (β) across the data sets in this study and β variations always should be taken into consideration when making characteristic lifetime comparisons between data sets. Alloy comparisons must also take into consideration that the actual, assembled solder compositions of all but the SAC305 test cell deviate from the nominal composition due to assembly with SAC305 solder paste, which has a greater effect on the smaller, 84CTBGA [12].

**Table 4:** Summary of the Weibull characteristic lifetime (η) and slope (β) data for the 192CABGA.

| 192CABGA ATC Data | | | |
|---|---|---|---|
| Solder Alloy | Temperature Cycle | Characteristic Lifetime η | Slope β |
| SAC405 | 0/100 °C | 6164 | 8.17 |
| | -40/125 °C | 1298 | 5.62 |
| SAC305 | 0/100 °C | 5718 | 6.99 |
| | -40/125 | 1611 | 6.52 |
| SAC205 | 0/100 °C | 5312 | 10.66 |
| | -40/125 °C | 1268 | 5.49 |
| SAC105 | 0/100 °C | 4910 | 5.40 |
| | -40/125 °C | 940 | 4.94 |
| SN100C | 0/100 °C | 3066 | 10.03 |
| | -40/125 °C | 826 | 7.95 |
| SnPb | 0/100 °C | 1477 | 12.39 |
| SnPb | -40/125 °C | 658 | 6.77 |

**Table 5:** Summary of the Weibull characteristic lifetime (η) and slope (β) data for the 84CTBGA.

| 84CTBGA ATC Data | | | |
|---|---|---|---|
| Solder Alloy | Temperature Cycle | Characteristic Lifetime η | Slope β |
| SAC405 | 0/100 °C | 11433 | 5.63 |
| | -40/125 °C | 2417 | 2.91 |
| SAC305 | 0/100 °C | 9819 | 7.05 |
| | -40/125 | 2430 | 5.83 |
| SAC205 | 0/100 °C | 9062 | 7.12 |
| | -40/125 °C | 2232 | 6.50 |
| SAC105 | 0/100 °C | 6826 | 7.87 |
| | -40/125 °C | 1581 | 3.85 |
| SN100C | 0/100 °C | 6625 | 8.00 |
| | -40/125 °C | 1682 | 5.09 |
| SnPb | 0/100 °C | 2381 | 11.01 |
| SnPb | -40/125 °C | 988 | 5.67 |

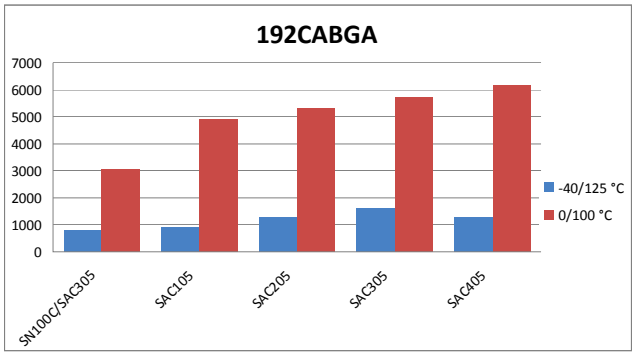


**Figure 3:** Bar chart comparing characteristic lifetime as a function of alloy composition (Ag content) and thermal cycle for the 192CABGA.

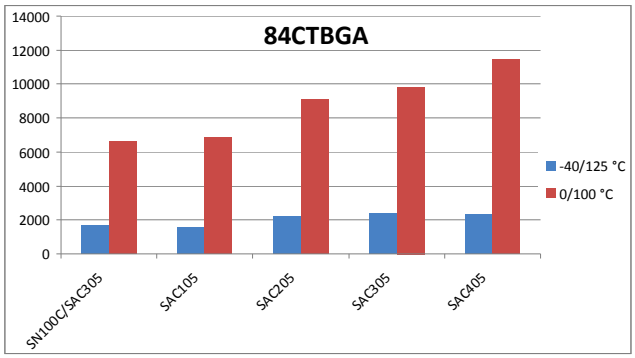


**Figure 4:** Bar chart comparing characteristic lifetime as a function of alloy composition (Ag content) and thermal cycle for the 84CTBGA.

The most obvious trend in these data is that the 84CTBGA outperforms the 192CABGA by 30-40% in characteristic lifetime across all alloys, including eutectic SnPb. This is true even though the die to package ratio is similarly large for both components (Table 2). The better reliability of the 84CTBGA may be attributed to the fact that the outer row of balls lies outside the die shadow, whereas the die shadow extends under the outer row in the 192CABGA. The 84CTBGA may also benefit from secondary effects resulting from its fine microstructural features (Figures 2a and 2b) and the increased Ag content derived from adding SAC305 paste to a smaller solder ball.

Figures 3 and 4 indicate that there is a general decrease in characteristic lifetime for the 192CABGA and 84CTBGA packages with decreasing alloy Ag content. The relationship between fatigue life and Ag content is more apparent with the 0/100 °C cycling and less noticeable with the -40/125 °C cycling.

In the 0/100 °C cycling the characteristic lifetimes for both packages with the SAC405 alloy (4 wt. % Ag) are approximately twice that for the SN100C (nominally zero Ag but with 0.3-0.8% Ag stemming from the SAC305 assembly paste). The differences in characteristic lifetime between SAC405 and SAC105 are 20% for the 192CABGA and 40% for the 84CTBGA. Less dependence on Ag content in the 192CABGA might be anticipated due to higher strain levels in this package. These trends are consistent with other data from the literature cited in the introduction section of this paper [4-9].

In -40/125 °C testing the dependence of characteristic lifetimes on Ag content is not as dramatic with either BGA package. While the SAC405 still is about 50% more reliable than the SN100C, the reduction in reliability with decreasing levels of Ag content is less obvious. In fact, it could be argued that there is minimal statistical difference in reliability between the various Sn based Pb-free alloys in the -40/125 °C test. This result is not surprising considering the recent results reported by Lee and Ma, in which they observed a minimal difference in performance between SAC305 and SAC105 using a high-stress test vehicle configuration [17]. They concluded that $Ag_3Sn$ precipitate coarsening occurred so rapidly under their test conditions that the Ag content and particle density were no longer the primary factors controlling thermal fatigue life. The results for the -40/125 °C cycle are consistent with the Lee and Ma hypothesis because this severe temperature cycle is characterized by a combination of the highest strain ($\triangle T$) and the highest upper temperature extreme. The observation that $\eta$ is sensitive to Ag content with the -40/125 °C profile also is consistent with the findings of Henshall et al. [25].

There is one trend in the -40/125 °C data that is considered unexpected or anomalous. Compared to the 0/100 °C cycle, -40/125 °C accelerates Pb-free fatigue failure much faster than expected. Rapid failures are expected with -40/125 °C testing, but the nominal acceleration factor for this cycle is almost 5 times faster than 0/100 °C in most of the Pb-free test cells. There are few direct comparisons in the literature for these two thermal cycles using area array components, but a lower acceleration factor of approximately 2-3.5 might be expected based on earlier work [18, 25]. In the current study, both of the component test vehicles are chip scale packages with very large die to package ratio, and perhaps the -40/125 °C cycle drives failures in these packages much faster than expected based on the limited previous test results.

On the other hand, the data for the eutectic Sn-37Pb shows a difference in acceleration between the two cycles of about 2 times, which is anticipated based on results from the literature [19, 25]. Tables 4 and 5 show that the $\beta$ values for the -40/125 °C data are significantly lower than those for the 0/100 °C data and this may be a factor to consider in interpreting these data.

For some time it has been hypothesized that the eutectic Sn-37Pb should outperform SAC in high strain environments [e.g., 20] which does not seem to be the case here. All the Sn based Pb-free alloys including the SN100C outperform eutectic Sn-37Pb despite the fact that both BGA components are considered to be high strain packages and the fact that the -40/125 °C test embodies high strain test conditions. This finding is largely consistent with earlier results [25].

## FAILURE ANALYSIS

Metallographic failure analysis was performed to confirm and document the solder joint thermal fatigue failures. The optical photomicrographs in Figure 5 show thermal fatigue cracking in the 192CABGA and 84CTBGA solder joints assembled with the five Pb-free solder alloys and the SnPb eutectic alloy. The fatigue damage typically is greater in the 192 CABGA due to the extended cycling beyond the final failure for that package. In both components, the most significant amount of damage was observed at the die shadow as expected for these package constructions. It is assumed that the initial failures occur at the package corners or at the die shadow but that can not be confirmed by the metallographic analysis.

Pb-free solder thermal fatigue cracking is characterized by a variety of crack paths and fracture features described as crack branching, recrystalization and cavitation. The fracture characteristics observed in these Pb-free alloys are seen routinely in SAC fatigue failures and are consistent with those reported much earlier by workers such as Dunford [21]. The fatigue cracking in the Sn-37Pb solder propagates between the Pb-rich and Sn-rich phases.

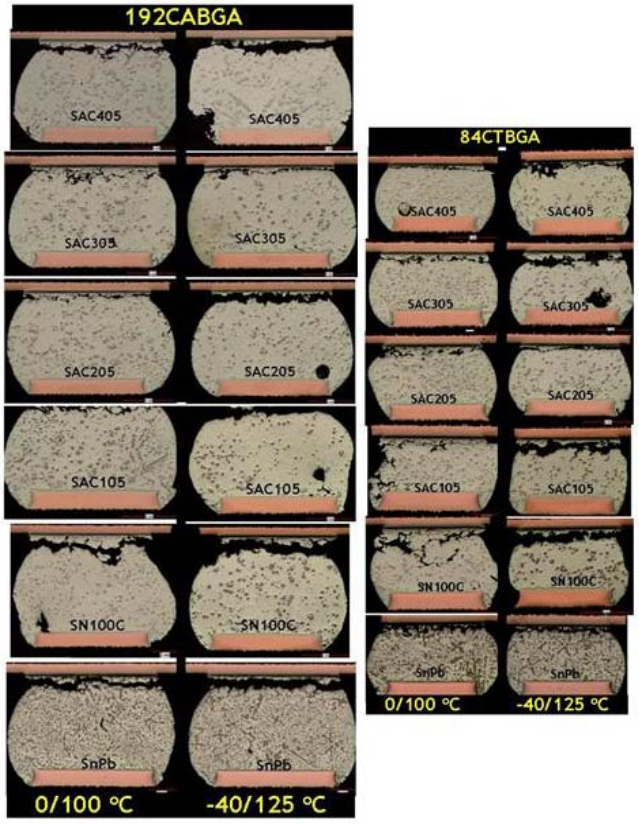


**Figure 5:** Thermal fatigue cracking in the 192CABGA and 84CTBGA solder joints assembled with the five Sn based Pb-free solders and the eutectic SnPb.

A limited amount of SEM analysis was performed on SAC305 and SAC105 solder joints for both temperature cycles. The electron micrographs in Figures 6 and 7 illustrate intermetallic particle coarsening in the highly strained region surrounding the fatigue cracking in both alloys and components. Strain-enhanced aging occurs during temperature cycling and accelerates particle coarsening and promotes fatigue crack propagation. The baseline microstructures are compared to those for both temperature cycling tests. With both temperature cycles, there are very few $Ag_3Sn$ particles in the strain-localized region surrounding the fatigue crack. Despite the significant differences in their thermal cycles, the resultant microstructures in these regions are very similar.

These preliminary findings appear to be consistent with data emerging from other segments of the iNEMI Alloy program [22] and support the hypothesis that Ag content is the most important factor in determining thermal fatigue reliability of this family of Sn based Pb-free solder alloys. However, there is some evidence in the literature that the Sn grain morphology and orientations of the anisotropic Sn grains can influence the fatigue behavior [23, 24]. Studying and characterizing the Sn orientation requires specialized analytical methods that are beyond the scope of the current study. Additional failure analysis for the other alloys possibly including advanced analytical methods will be presented in future publications.

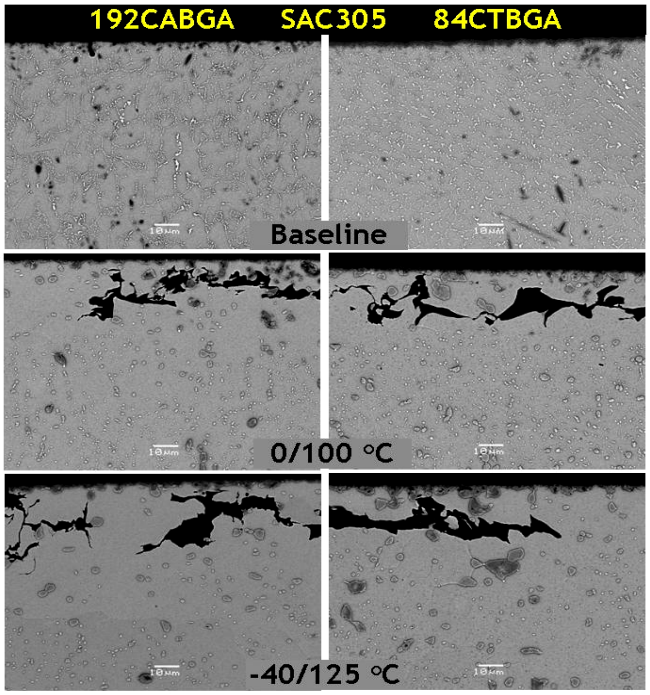


**Figure 6:** Backscattered electron micrographs showing the microstructural evolution and thermal fatigue cracking in the SAC305 192CABGA and 84CTBGA solder joints.

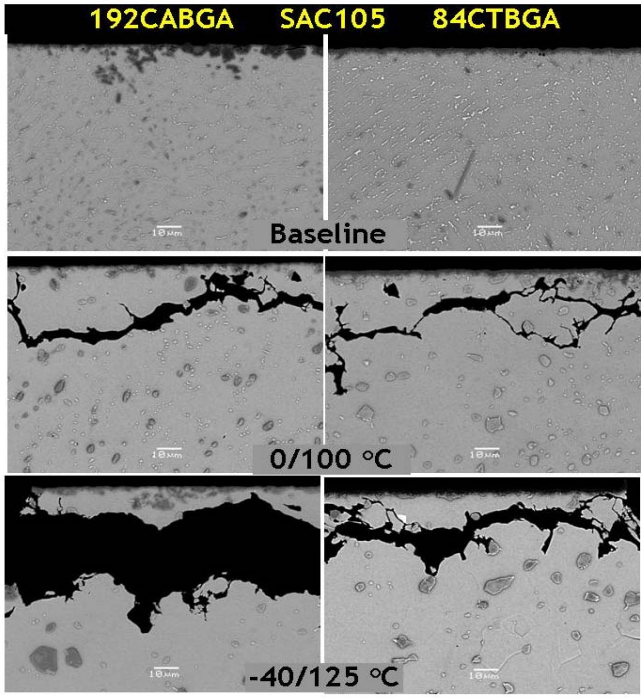


**Figure 7:** Backscattered electron micrographs showing the microstructural evolution and thermal fatigue cracking in the SAC105 192CABGA and 84CTBGA solder joints.

## SUGGESTIONS FOR FUTURE WORK

Further failure analysis and microstructural characterization is recommended in order to understand the large acceleration difference between the -40/125 °C and 0/100 °C temperature cycles. Specialized techniques for microstructural characterization could be explored including polarized light microscopy (PLM) and orientation image microscopy (OIM) using electron backscattered diffraction (EBSD). Extended thermal cycling may cause sample damage that will limit the effectiveness of either of these techniques. If that is the case, some advanced microstructural analysis on the baseline samples may provide some insight relative to the failure behavior in the various alloys.

## SUMMARY AND CONCLUSIONS

Accelerated temperature cycling was used to compare the thermal cycling performance of multiple Pb-free solder alloys using two of the most commonly specified temperature cycles, 0/100 °C and -40/125 °C. The experimental test matrix included two different component test vehicles, five different Sn based Pb-free alloys, and a eutectic Sn-37Pb control. The following observations and conclusions can be drawn from the results of this study.

- In general, the characteristic fatigue lifetime for the 192CABGA and 84CTBGA packages decreases with decreasing alloy Ag content. The relationship between fatigue life and Ag content is very apparent with the 0/100 °C cycling but much less evident with the -40/125 °C cycling.
- The -40/125 °C cycle accelerated thermal fatigue failures in the Pb-free solders almost 5times faster than the 0/100 °C cycle. A lower acceleration factor of approximately 2-3.5 was anticipated based on limited information from the literature.
- The data for the Sn-37Pb shows a difference in acceleration between the two cycles of about 2 times, which is aligned with results from the literature.
- All the Sn based Pb-free alloys including the SN100C outperform the Sn-37Pb. This finding contradicts the common proposition that Sn-37Pb solder will outperform Sn based Pb-free solders when used in high strain packages and tested under high strain conditions such as the -40/125 °C cycle. The performance gap between the Sn-37Pb and Pb-free solders may decrease if the test dwell time is increased. The test matrix for this iNEMI Alloy Program includes testing with longer dwell times and those results will be published at a later date.

## ACKNOWLEDGEMENTS

The authors want to acknowledge the continued guidance of iNEMI, particularly that of David Godlewski and Jim Arnold. The authors also thank Keith Sweatman and Keith Howell of Nihon Superior and Liang Yin of Universal Instruments for numerous helpful technical discussions. Many thanks to Pete Read and Debra Fleming from Alcatel-Lucent for helpful technical discussions, metallographic characterization, and failure analysis.

The authors thank Jim Carrigan, Dave Grant, and the entire staff at Premier Semiconductor Services LLC for their flawless execution of balling the test packages. Thanks to Jason Bragg of Celestica for analyses related to samples from the Premier process to ensure integrity of the ball attachments.

Many thanks to Jon Goodbread of Agilent Technologies for his efforts in developing the DAS code for the Agilent data acquisition systems. We wish to thank Richard Popowich of Alcatel-Lucent and Raul Zubia, Jesus Moreno, and Jose Valdes of Delphi for their efforts towards the ATC setup and execution.

## REFERENCES

[1] Gregory Henshall, "Lead-free Alloys for BGA/CSP Components," in **Lead-free Solder Process Development**, 95-124, IEEE Press, John Wiley ands Sons, 2011.

[2] Gregory Henshall, Keith Sweatman, Keith Howell, Joe Smetana and Richard Coyle, Richard Parker, Stephen Tisdale, Fay Hua, Weiping Liu, Robert Healey, Ranjit S. Pandher, Derek Daily, Mark Currie, Jennifer Nguyen, "iNEMI Lead-Free Alloy Alternatives Project Report: Thermal Fatigue Experiments and Alloy Test Requirements," *Proceedings of SMTAI*, 317-324, San Diego CA, 2009.

[3] Werner Engelmaier "Surface Mount Solder Joint Long-Term Reliability: Design, Testing, Prediction," *Soldering and Surface Mount Technology*, vol. 1, no. 1, 14-22, February, 1989.
[4] Richard Coyle, John Osenbach, Maurice Collins, Heather McCormick, Peter Read, Debra Fleming, Richard Popowich, Jeff Punch, Michael Reid, and Steven Kummerl, "Phenomenological Study of the Effect of Microstructural Evolution on the Thermal Fatigue Resistance of Pb-Free Solder Joints," *IEEE Trans. CPMT*, vol. 1, no. 10, 1583-1593, October 2011.
[5] Richard Coyle, Peter Read, Heather McCormick, Richard Popowich, and Debra Fleming, "The Influence of Alloy Composition and Temperature Cycling Dwell Time on the Reliability of a Quad Flat No Lead (QFN) Package," *Journal of SMT*, Vol. 25, Issue 1, 28-34, January-March 2011.
[6] Richard Coyle, Heather McCormick, John Osenbach, Peter Read, Richard Popowich, Debra Fleming, and John Manock, "Pb-free Alloy Silver Content and Thermal Fatigue Reliability of a Large Plastic Ball Grid Array (PBGA) Package," *Journal of SMT*, Vol. 24, Issue 1, 27-33, January-March 2011.
[7] Richard Coyle, Robert Kinyanjui, Peter Read, Jonathon Shirey, Debra Fleming, Mulugeta Abtew, Richard Popowich, Iulia Muntele, and John Manock, "Solder Joint Reliability of Pb-Free Tin-Silver-Copper Ceramic Ball Grid Array (CBGA) Packages as a Function of Cooling Rate and Silver Content," *Proceedings of SMTAI 2010*, 548-558, Orlando, FL, October 2010.
[8] G. Henshall. J. Bath, S. Sethuraman, D. Geiger, A. Syed, M.J. Lee, K. Newman, L. Hu, D. Hyun Kim, Weidong Xie, W. Eagar, and J. Waldvogel, "Comparison of Thermal Fatigue Performance of SAC105 (Sn-1.0Ag-0.5Cu), Sn-3.5Ag, and SAC305 (Sn-3.0Ag-0.5Cu) BGA Components with SAC305 Solder Paste," *Proceedings APEX*, S05-03, 2009.
[9] S. Terashima, Y. Kariya, Hosoi, and M. Tanaka, "Effect of Silver Content on Thermal Fatigue Life of Sn-xAg-0.5Cu Flip-Chip Interconnects," *J. Electron. Mater.* vol. 32, no. 12, 2003.
[10] Jean-Paul Clech, Gregory Henshall, and Jian Miremadi, "Closed-Form, Strain-Energy Based Acceleration Factors for Thermal Cycling of Lead-Free Assemblies," *Proceedings of the SMTAI 2009,* 393-408, October, 2009.
[11] G. Henshall, R. Healy, R. S. Pander, K. Sweatman, K. Howell, R. Coyle, T. Sack, P. Snugovsky, S. Tisdale, and F. Hua, "iNEMI Pb-free Alloy Alternatives Project Report: State of the Industry, *SMTJournal*, vol. 21, no. 4, 11, 2008.
[12] Gregory Henshall, Jian Miremadi, Richard Parker, Richard Coyle, Joe Smetana, Jennifer Nguyen, Weiping Liu, Keith Sweatman, Keith Howell, Ranjit S. Pandher, Derek Daily, Mark Currie, Tae-Kyu Lee, Julie Silk, Bill Jones, Stephen Tisdale, Fay Hua, Michael Osterman, Bill Barthel, Thilo Sack, Polina Snugovsky, Ahmer Syed, Aileen Allen, Joelle Arnold, Donald Moore, Graver Chang, and Elizabeth Benedetto, "iNEMI Pb-Free Alloy Characterization Project Report: Part I – Program Goals, Experimental Structure, Alloy Characterization, and Test Protocols for Accelerated Temperature Cycling," *Proceedings of SMTAI 2012*, Orlando, FL, October 2012.
[13] IPC-9701A, "Performance Test Methods and Qualification Requirements for Surface Mount Solder Attachments," IPC, Bannockburn, IL, 2006.
[14] R. Kinyanjui, L. P. Lehman, L. Zavalij, and E. Cotts, "Effect of sample size on the solidification temperature and microstructure of SnAgCu near eutectic alloys," *J. Materials Research*, Vol. 20, No. 11, 2914-2918, November 2005.
[15] Liang Yin, Luke Wentlent, LinLin Yang, Babak Arfaei, Awni Oasaimeh, and Peter Bargemen, "Recrystallization and Precipitate Coarsening in Pb-Free Solder Joints During Thermomechanical Fatigue," J. Electronic Materials, Vol. 41, No. 2, 241-252, 2011.
[16] L. Snugovsky, P. Snugovsky, D.D. Perovic, and J. W. Rutter, "Spalling of SAC Pb free solders when used with Ni substrates," Materials Science and Technology, vol. 25, no. 10, 1296-1300, 2009.
[17] Tae-Kyu Lee and Hongtao Ma, "Aging Impact on the Accelerated Thermal Cycling performance of lead-Free BGA Solder Joints in Various Stress Conditions," *Proceedings of Electronic Components and Technology Conference,* 477-482, San Diego, CA, May 29- June 1, 2012.
[18] J. Manock, R. Coyle, B. Vaccaro, H. McCormick, R. Popowich, D., P. Read., J. Osenbach, and D. Gerlach, "Effect of Temperature Cycling Parameters on the Solder Joint Reliability of a Pb-free PBGA Package," *SMT J.*, vol. 21, no.3, 36, 2008.
[19] V. S. Sastry, J. C. Manock, and T. I. Ejim, "Effect Of Thermal Cycling Ramp Rates On Solder Joint Fatigue Life," *Proceedings of the SMTAI 2000,* 331-336, September, 2000.
[20] J. Smetana, J., R. Coyle, T. Sack, A. Syed, D. Love, D. Tu, S. Kummerl, "Pb-free Solder Joint Reliability in a Mildly Accelerated Test Condition," *Proceedings of IPC/APEX*, Las Vegas, NV, April 2011.
[21] S. Dunford, S. Canumalla, and P. Viswanadham, "Intermetallic Morphology and Damage Evolution Under Thermomechanical Fatigue of Lead (Pb)-Free Solder Interconnections," *Proceedings of Electronic Components Technology Conference,* 726-736, Las Vegas, NV, June 1-4, 2004.
[22] Richard Coyle, Richard Parker, Gregory Henshall, Michael Osterman, Joe Smetana, Elizabeth Benedetto, Donald Moore, Graver Chang, Joelle Arnold, and Tae-Kyu Lee, iNEMI Pb-Free Alloy Characterization Project Report: Part IV - Effect of Isothermal Preconditioning on Thermal Fatigue Life," *Proceedings of SMTAI 2012*, Orlando, FL, October 2012.
[23] B. Arfaei, N. Kim, and E.J. Cotts, "Dependence of Sn Grain Morphology of Sn-Ag-Cu Solder on Solidification Temperature," J. Electronic Materials, Published online Oct 19, 2011.
[24] Liang Yin, Luke Wentlent, LinLin Yang, Babak Arfaei, Awni Oasaimeh, and Peter Bargemen, "Recrystallization and Precipitate Coarsening in Pb-Free Solder Joints During Thermomechanical Fatigue," J. Electronic Materials, Vol. 41, No. 2, 241

[25] Gregory Henshall, Michael Fehrenbach, Chrys Shea, Quyen Chu, Girish Wable, Ranjit Pandher, Ken Hubbard, Gnyaneshwar Ramakrishna, Ahmer Syed, "Low-Silver BGA Assembly, Phase II – Reliability Assessment. Sixth Report: Thermal Cycling Results for Unmixed Joints," *Proceedings of SMTAI 2010*, 595-606, Orlando, FL, October 2010.

# APPENDIX A

**Optical Photomicrographs of Surface Mount Assembled 192CABGA and 84CTBGA Samples**

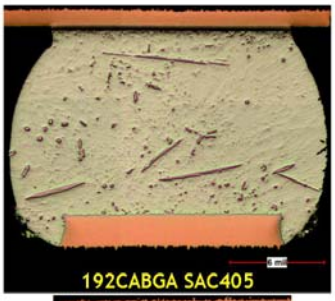


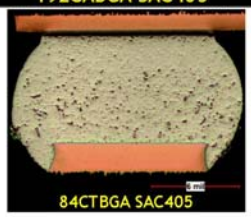


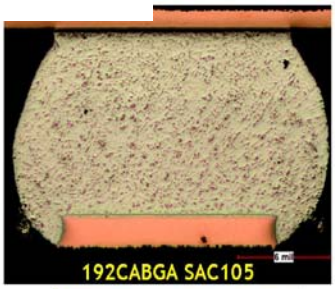


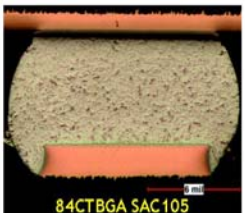




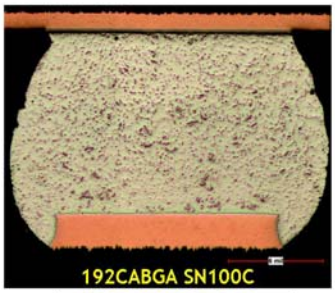


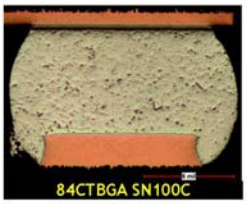



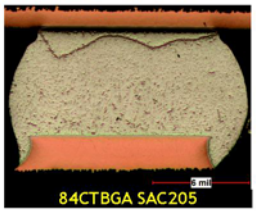



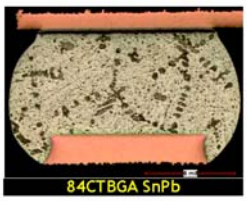

# APPENDIX B

## Weibull and Contour Plots